Teleconnected Influence of the Boreal Winter Antarctic Oscillation on the Somali Jet: Bridging Role of Sea Surface Temperature in Southern High and Middle Latitudes

Wenjing SHI[1,2,4], Ziniu XIAO[*1,2], and Jianjun XUE[3]

[1]*Department of Atmospheric Science, Nanjing University of Information Science & Technology, Nanjing* 210044
[2]*State Key Laboratory of Numerical Modeling for Atmospheric Sciences and Geophysical Fluid Dynamics, Institute of Atmospheric Physics, Chinese Academy of Sciences, Beijing* 100029
[3]*Training Center, China Metrological Administration, Beijing* 100081
[4]*Cooperative Institute for Meteorological Satellite Studies, University of Wisconsin–Madison, Madison, WI* 53706, *USA*

(Received 13 April 2015; revised 30 May 2015; accepted 16 June 2015)

ABSTRACT

The teleconnection impact of the boreal winter Antarctic Oscillation (AAO) on the Somali Jet (SMJ) intensity in the following spring and summer is examined in this paper. The variability of the boreal winter AAO is positively related to the SMJ intensity in both spring and summer. The analyses show that the SST in southern high and middle latitudes seems to serve as a bridge linking these two systems. When the AAO is in strong positive phase, SST over the Southern Ocean cools in the high latitudes and warms in the middle latitudes, which persists into summer; however, the variability of SST in southern high and middle latitudes is also closely correlated to SMJ intensity.

A possible mechanism that links SST variability with the AAO–SMJ relationship is also discussed. The AAO in boreal winter produces an SST anomaly pattern in southern high and middle latitudes through the air–sea coupling. This AAO-related SST anomaly pattern modulates the local Ferrel cell anomaly in summer, followed by the regional Hadley cell anomaly in tropics. The anomalous vertical motion in tropics then changes the land–sea thermal contrast between the tropical Indian Ocean and the Asian continent through the variability of low cloud cover and downward surface longwave radiation flux. Finally, the land–sea thermal contrast anomaly between the tropical Indian Ocean and the Asian continent changes the SMJ intensity. The results from Community Atmosphere Model experiments forced by the SST anomaly in southern high and middle latitudes also confirm this diagnostic physical process to some extent.

Key words: Antarctic Oscillation, Somali Jet intensity, teleconnection influence, sea surface temperature, longwave radiation flux

Citation: Shi, W. J., Z. N. Xiao, and J. J. Xue, 2016: Teleconnected influence of the boreal winter Antarctic Oscillation on the Somali Jet: Bridging role of sea surface temperature in southern high and middle latitudes. *Adv. Atmos. Sci.*, **33**(1), 47–57, doi: 10.1007/s00376-015-5094-7.

1. Introduction

In boreal summer, equatorial regions are characterized by large-scale northward cross-equatorial flows (CEFs), of which the Somali Jet (SMJ) (Findlater, 1969; Krishnamurti and Bhalme, 1976) is the strongest and largest. This jet originates from the Mascarene High and Australian High in the SH and turns anticyclonically in the NH, resulting in westerlies that sweep over the Indian Peninsula. Its peak low-level wind speeds typically occur near the east coast of Somalia. The factors involved in the variability and formation of the SMJ have been studied based on statistical and simulation techniques since Findlater (1969) discovered this CEF. Using a one-level primitive equation model that incorporated detailed orographic features of the east African mountains, Krishnamurti et al. (1976) highlighted the importance of the land–sea thermal contrast, East African mountains, and beta effect on the simulation of the SMJ. Besides, in the simulations of Chakraborty et al. (2009), the SMJ occurred even in the absence of African orography, which only strengthened the CEFs; the longitudinal location of the jet depends on the diabatic heating of the Indian monsoon, while the vertical structure depends on the western boundary current due to the East African highlands.

As an important component of the Asian summer mon-

* Corresponding author : Ziniu XIAO
Email: xiaozn@lasg.iap.ac.cn

soon system, the SMJ is usually connected to Indian summer monsoon rainfall as well as rainfall in China. Commonly, positive relationships are seen between the SMJ strength and the amount of rainfall in most regions of India, especially in the monsoon regions at both interannual and interdecadal timescales (Halpern and Woiceshyn, 2001; Cong et al., 2007). In fact, the energy of the SMJ may be dispersed northeastwards, bringing large amounts of water vapor to the East Asian summer monsoon (EASM) regions (Wang and Xue, 2003; Shi and Xiao, 2013; Dai and Xiao, 2014), but only a minor relationship is found between the SMJ and EASM rainfall (Lei and Yang, 2008; Zhu, 2012). Instead, the Australian CEFs, another set of CEFs to the east of the SMJ, play an important role in the EASM rainfall and rainfall over China (Zhu, 2012; Li and Li, 2014).

As a leading mode of the extratropical atmosphere in the SH, the Antarctic Oscillation (AAO) has become a focus of attention recently. The AAO is a "seesaw" pattern between the pressures or geopotential heights in the subtropics and higher latitudes. Many studies have verified that the AAO variability is not only associated with the climate systems at high and middle latitudes of the SH (e.g., Ummenhofer et al., 2008), but also relates to the climate in the NH. For example, strong positive AAO events in spring are followed by a weak EASM, and vice versa (Nan and Li, 2003; Gao et al., 2003). Ho et al. (2005) also showed that the large-scale atmospheric circulation in the SH, which is related to the AAO variability, might modulate tropical cyclone activity in the western North Pacific during the typhoon season. Besides, as pointed out by Gao et al. (2013), the AAO in boreal winter has a significant precursory influence on the timing of the Asian summer monsoon onset. They suggested that in stronger AAO years, both the Mascarene High and Australian High in March are stronger owing to the "seesaw" circulation structure over the southern subtropics and higher latitudes, and the ITCZ is enhanced. Thus, the pressure gradient between the subtropical and tropical regions increases and accelerates the establishment of the SMJ in spring, resulting in an accelerating onset of the Asian summer monsoon.

The above works show that the SMJ plays a bridging role in the effects of the AAO on the climate in the NH or on the monsoons. Thus, it is meaningful to verify the hypothesis that the remote southern atmospheric oscillation may also significantly affect the variability of the SMJ strength in tropical regions. And if a relationship exists between these two components, what is the possible physical process involved? Addressing these aspects could provide useful information on precursory signals when attempting to predict the monsoon climate in an operational setting. The paper is organized as follows: Details about the dataset and methods used are described in section 2, followed by an examination of the relationship between the SMJ strength and AAO in section 3. The possible linkage mechanism is discussed in section 4, based on both statistical and simulation analysis. Finally, a summary of the study's key findings is provided in section 5.

2. Data and methods

Several datasets are used in this paper. The monthly mean atmospheric reanalysis dataset with a resolution of $2.5^\circ \times 2.5^\circ$ is from the National Centers for Environmental Prediction–National Center for Atmospheric Research (NCEP–NCAR) (Kalnay et al., 1996) for the period 1951–2012. The variables include horizontal wind (u and v), surface air temperature (SAT), sea level pressure (SLP), and vertical velocity (ω). Monthly mean SST data are from National Climatic Data Center Extended Reconstructed SST dataset (Smith and Reynolds, 2004), with a $2^\circ \times 2^\circ$ resolution and covering the period 1951–2012. Because of the slow process of change in the ocean, we also use the monthly subsurface ocean temperature from version 2.1.6 of the Simple Ocean Data Assimilation reanalysis for the period 1958–2008, with a $0.5^\circ \times 0.5^\circ \times 40$-level grid (Carton et al., 2000a, b). The interpolated outgoing longwave radiation (OLR) data on a $2.5^\circ \times 2.5^\circ$ grid, used to infer tropical convection, are provided by the National Oceanic and Atmospheric Administration (NOAA), and are available from June 1974 onward with a missing period between March and December in 1978 (Gruber and Krueger, 1984). The surface radiation fluxes and low cloud cover on a $2.5^\circ \times 2.5^\circ$ grid from ERA-40 (the European Center for Medium-Range Weather Forecasts 40-yr Reanalysis) (Uppala et al., 2005) cover the period 1958–2002. Meanwhile, the surface radiation fluxes on the Gaussian grid (192×94) from the NCEP–NCAR reanalysis cover the period 1951–2012. To confirm the results diagnosed from the observational and reanalysis data, version 5 of the Community Atmosphere Model (CAM5) (Neale et al., 2010) is used.

The SMJ intensity index (SMJI) is defined as the area-averaged meridional wind speed over SMJ regions (40°–55°E at the equator) from the surface to 700 hPa (Shi and Xiao, 2014). It is calculated by using the NCEP–NCAR reanalysis data for the period 1951–2012. The AAO index (or SH Annular Mode Index) (1951–2012) is the difference in the normalized zonal-mean SLP (from NCEP–NCAR) between 40°S and 70°S (Nan and Li, 2003), which is modified based on the AAO index defined by Gong and Wang (1999). The Niño3.4 index is adapted from NOAA's Climate Prediction Center for 1951–2012. The basic methods used include composite, simultaneous and lead–lag correlation analyses. The high and low cases of composite analysis are selected based on the fluctuations of the index beyond one standard deviation. The Student's $t-$test is applied for checking the significance of the results.

3. Relationships between SMJ intensity and boreal winter AAO

3.1. *SMJ intensity and AAO*

Figure 1a shows the normalized time series of the SMJI in spring (March–May, MAM) and summer (June–August, JJA) and the AAO index in boreal winter (December–February, DJF). The temporal variations of these three indices are gen-

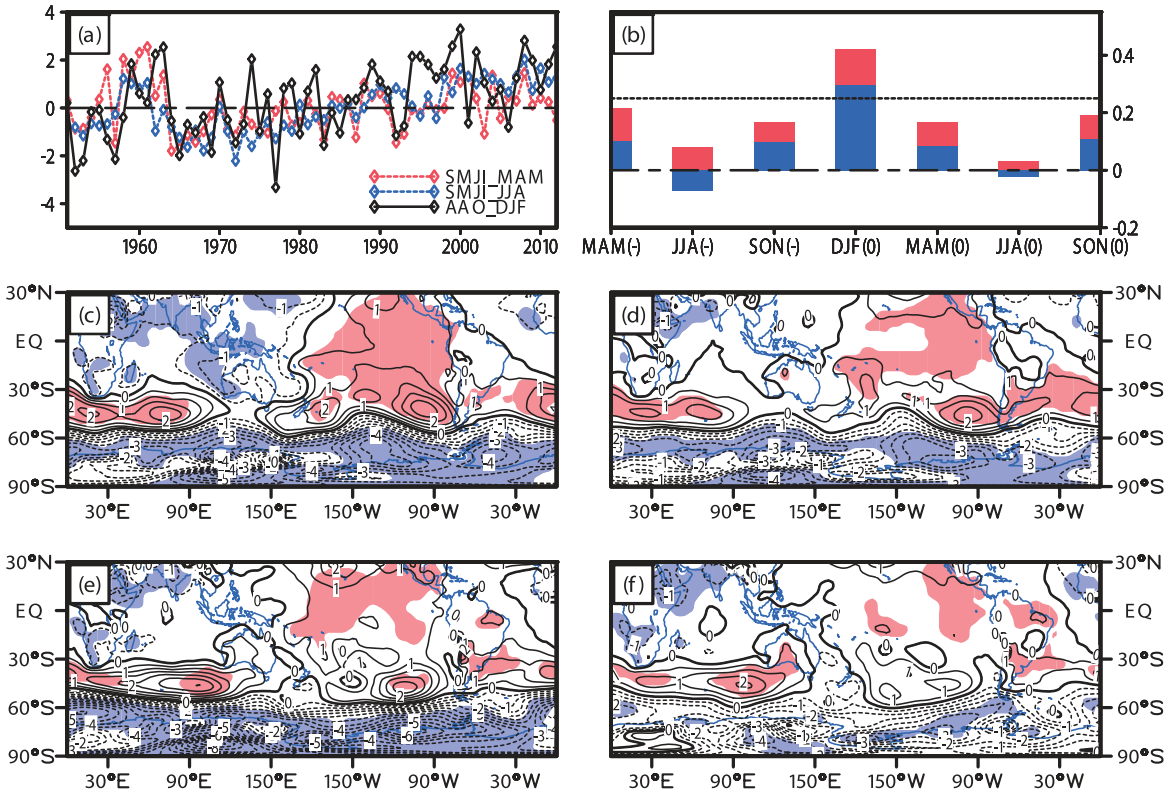

Fig. 1. (a) Normalized time series of SMJI in spring (red dashed line) and summer (blue dashed line) and AAO index in winter (black solid line). (b) Lead–lag correlation of spring (red bars) and summer (blue bars) SMJI with the seasonal AAO index. A minus sign after the season abbreviation, e.g., MAM(−), represents the preceding season, while a zero, e.g., DJF(0), represents the following season. The dashed line indicates correlation coefficients significant at the 95% confidence level. Composite differences of the winter SLP (units: hPa) between the high and low (c) spring and (e) summer SMJI cases. (d, f) As in (c, e) but with the ENSO signals removed. The red and blue shaded areas are significant at the 95% confidence level for positive and negative differences, respectively. The counter interval is 0.5 hPa.

erally in phase, which is stronger around 1960 and after the mid-1980s but weaker during the intervening period. As we know, the positive trends in the SMJI and AAO are significant in recent decades (Thompson and Wallace, 2000; Hoerling et al., 2004; Gao et al., 2013; Shi and Xiao, 2014). From calculations, we find that the increasing trends of the SMJI in summer and the AAO index in winter are significant at the 99% confidence level; thus, linear trends are removed from all statistical analysis datasets in this paper in order to isolate the contribution of the trends from that of natural variability (Nan et al., 2009).

To confirm the important impact of the AAO on the SMJ intensity in subsequent seasons, we calculate the lead–lag correlation of the SMJI in spring and summer with the seasonal average AAO index (Fig. 1b). Significant correlation only appears in the correlation with the winter AAO, with values of 0.422 and 0.278 for spring and summer SMJI (Table 1), respectively, which are beyond the 95% confidence level. However, after removing ENSO-related signals, the correlation coefficients of spring and summer SMJI with preceding winter AAO index are still pronounced, with values of 0.314 and 0.364 (Table 1), respectively, which become slightly smaller for spring SMJI but larger for summer SMJI.

Table 1. Correlation coefficients between MAM/JJA SMJI and DJF AAO and simultaneous correlation coefficients of MAM/JJA SMJI with zonal-mean SST index (ZSSTI) in spring and summer for the period 1951–2012. Bold font indicates significance at the 95% confidence level. Bold and italic font indicates significance at the 99% confidence level. Values in brackets represent the results when the ENSO-related signals are removed.

	MAM SMJI	JJA SMJI
DJF AAO	**0.422(0.314)**	**0.278(0.364)**
ZSSTI	**0.445(0.388)**	**0.25(0.281)**

The composite differences of the SH SLP anomalies in winter between the high and low spring (summer) SMJI cases are presented in Fig. 1c (Fig. 1e). The 10 (6) highest spring (summer) SMJI years are 1956, 1958, 1959, 1960, 1961, 1963, 1999, 2001, 2004, and 2008 (1958, 1959, 1960, 1961, 2000 and 2008). The 12 (10) lowest spring (summer) SMJI years are 1957, 1964, 1965, 1966, 1967, 1972, 1976, 1983, 1987, 1992, 1993 and 2003 (1966, 1968, 1969, 1972, 1974, 1975, 1977, 1979, 1995 and 1997). The significant positive values cover the southern middle latitudes at 30°–50°S, while the significant negative values dominate over the South

Pole regions beyond 60°S. These two patterns over the southern extratropical regions resemble the feature of the positive AAO phase. Many previous studies have suggested that the SMJ and AAO demonstrate various correlations with ENSO (Chen et al., 2005; Nan et al., 2009; Zheng and Li, 2012; Zhu, 2012). The positive SLP anomalies in the equatorial central-eastern Pacific are noticeable in the composite result for the strong spring and summer SMJI cases (Figs. 1c and e). To sort out the relationships among the SMJI, ENSO and AAO, we remove the ENSO-related signals in both the SMJ intensity and SLP using linear regression analysis. The recalculated composite differences of winter SLP anomalies between strong and weak SMJI cases are shown in Fig. 1d for spring SMJI and Fig. 1f for summer SMJI. The procedures for removing the ENSO-related signals (Li and Li, 2014) used in our analysis are as follows: First, the ENSO-induced anomaly is determined by using the regression between the interannual time series of the SMJI, together with the SLP in each grid, and the Niño3.4 index time series. Second, the original interannual SMJI (SLP) minus the ENSO-induced anomaly yields the ENSO-removed SMJI (SLP). After removing ENSO-related signals, the remaining general patterns of winter SLP anomalies are similar to the raw ones but with a remarkable decrease in the positive SLP anomalies in the equatorial central-eastern Pacific. This implies that the winter AAO is a main cause of the influence of the SMJ intensity in the following spring and summer, and is independent of the ENSO signal.

3.2. *Bridging role of SST over southern high and middle latitudes in the AAO–SMJ relationship*

The next important question is how the boreal winter AAO influences the SMJ intensity in the following spring and summer. The ocean is known for having a "memory" to store and then release climatic signals. It seems to play an important role in transporting the signal from winter to summer. Our previous work also revealed that the southern SST anomalies may act as an "oceanic bridge" in this physical process (Shi and Xiao, 2014). More detailed analysis of the role of the southern SST anomaly will be carried out in the following subsection.

Previous studies (Wu et al., 2009; Zheng and Li, 2012) suggest that a strong positive phase of the AAO in winter is followed by warmer SST anomalies over the ocean in the southern midlatitudes but colder SST anomalies over the southern high latitudes, and vice versa. Here, similar results are presented. Correlations between the winter AAO index and southern SST anomalies in winter, spring and summer are shown in Figs. 2a–c. The large-scale significant positive correlations appear over the southern midlatitudes from 30°S to 45°S but negative ones occur over high latitudes from 50°S to 65°S. In fact, this correlation pattern can persist into the following summer. Although the correlations become weaker in the following spring and summer, the pattern is similar. For convenience of analysis, (ZSSTI) is defined following Zheng and Li (2012), which is the normalized differences of the zonal-mean SST over 30°–45°S and 50°–65°S. A positive (negative) ZSSTI means the zonal-mean SST over 30°–45°S is warmer (colder) than that over 50°–65°S.

To begin, lead–lag correlation is employed to analyze the relationship between the different seasonal AAO index values and the 3-month moving-mean ZSSTI. As shown in Fig. 3a, for the AAO index, significant correlations emerge in the preceding autumn (September–November, SON) and reach a maximum value of larger than 0.6 in winter, while the relationship between winter AAO index and the ZSSTI can persist into the following summer. This is consistent with the results shown in Fig. 2. Because the ocean is essentially a large energy container holding the climatic signal, anomalous signals may be clearly seen under the ocean's subsurface. Vertical profiles of the relationships between winter AAO index and the differences of the zonal-mean subsurface ocean temperature over 30°–45°S and 50°–65°S in winter, the following spring and summer are provided in Fig. 3b. Significant positive values exist above the depth of 35.76 m below the sea

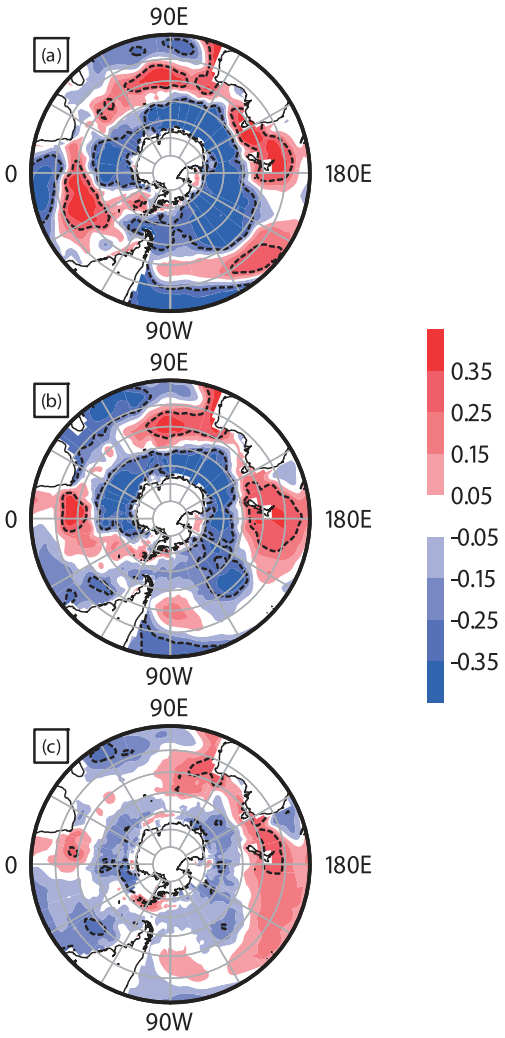

Fig. 2. Correlations between the winter AAO index and SST anomalies over the Southern Ocean in (a) winter and the (b) following spring and (c) summer. Areas circled by thick dashed curves are significant values exceeding the 95% confidence level.

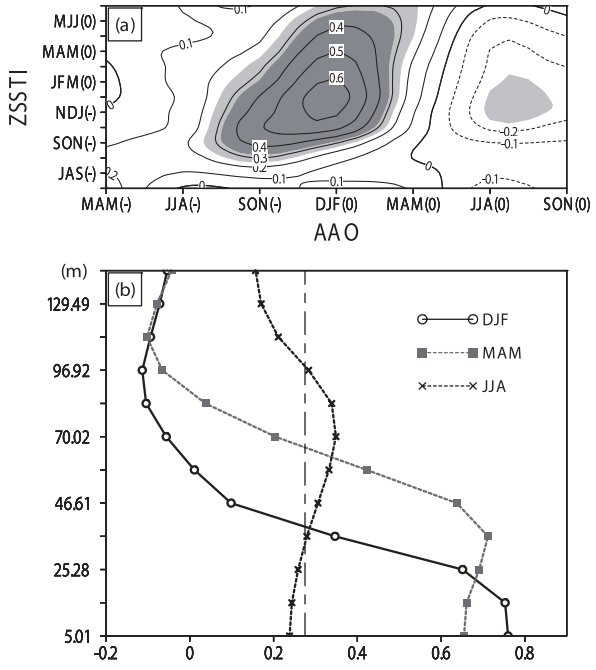

Fig. 3. (a) Lead–lag correlations of the seasonal AAO index with a 3-month moving mean ZSSTI. A minus sign after the season abbreviation, e.g., MAM(−), represents the preceding season, while a zero, e.g., DJF(0), represents the following season. Light and dark shading indicates significant values exceeding the 95% and 99% confidence level, respectively. The contour interval is 0.1. Positive, negative and zero contours are drawn with solid, dashed and thick lines, respectively. (b) Vertical profiles of the relationships between winter AAO index and differences of the zonal mean subsurface ocean temperature over 30°–45°S and 50°–65°S in winter (DJF; black solid line with circles) and the following spring (MAM; gray dashed line with squares) and summer (JJA; black dashed line with crosses). The *x*-axis is the depth below the sea surface level and the y-axis is the correlation coefficient. The dot-dashed line is the 95% confidence level.

surface level during winter, with a maximum correlation coefficient value of 0.76 at the depth of 5.01 m. In comparison, significant correlations are located above the depth of 57.98 m in spring, with a maximum correlation coefficient value of 0.71 at 35.76 m. For summer, significant values reach as deep as 96.92 m below the sea surface level, with a maximum correlation coefficient value of 0.34 at 70.02 m. The significant (or maximum) correlation coefficients become deeper with time from winter to summer. This indicates that the anomalous signals caused by the winter AAO pattern are stored in the ocean from winter and continue to remain in the following seasons.

The above analyses endorse the hypothesis that SST anomalies at southern high and middle latitudes are connected to the AAO events of the preceding winter. How closely the SMJI variability is related to SST anomalies over the southern ocean is also investigated. The ZSSTI is a better measure for presenting the dipole pattern. The simultaneous correlation coefficients between the SMJI and ZSSTI in spring and summer are 0.445 and 0.25, respectively; both exceed the 95% confidence level, even with ENSO-related signals removed (the values in brackets shown in Table 1). This indicates that the strengthened SMJ is associated with the warmer SST in the southern midlatitude ocean and cooler SST in the southern high-latitude ocean, and vice versa. It is important to note that these features are similar to those demonstrated by the AAO–ZSSTI relationship in Figs. 2 and 3. In summary, when the boreal winter AAO is in strong positive phase, a dipole-like SST anomaly pattern will occur, with a positive anomaly over the southern midlatitude ocean and a negative anomaly over the southern high-latitude ocean. The pattern persists from boreal winter to the following summer and impacts upon the SMJ intensity in spring and summer. Therefore, the southern high- and midlatitude SST is associated with the SMJ and AAO, which plays an important bridging role in the SMJ–AAO relationship. In fact, the correlation of the AAO with the SMJ intensity in spring is similar to that in summer, which may be attributable to the seasonal persistence of the SMJ intensity (the correlation coefficient between the SMJI in spring and that in summer is 0.6, exceeding the 99% confidence level). Because summer SMJ variability has a more important impact on Asian climate, analysis of the summer season only is carried out hereinafter.

4. The role of the ocean in the possible linkage mechanism

4.1. *Statistical analysis results*

So, what is the potential physical process involved in the SST anomalies over the southern high and middle latitudes being responsible for the SMJ–AAO relationship? To examine this, the SAT, surface heat fluxes and atmospheric circulations are analyzed using composite and correlation analysis. The composite approach is used to analyze the difference between the strong and weak ZSSTI years. For the period 1951–2012, 13 low summer-ZSSTI cases occur in 1965, 1966, 1969, 1977, 1980, 1981, 1982, 1983, 1991, 1992, 1993, 1994 and 1996, while 13 high summer-ZSSTI cases occur in 1951, 1955, 1957, 1959, 1962, 1972, 1974, 2004, 2007, 2008, 2010, 2011, and 2012.

As Rodwell and Hoskins (1995) verified using a primitive equation model, the land–sea thermal contrasts caused by orography play an important role in the variability of the SMJ strength. Composite differences of SAT and (*u*, *v*) at 850 hPa between the high and low summer-ZSSTI cases are presented in Fig. 4. It can be seen from Fig. 4a that there are large-scale negative values covering the whole tropical Indian Ocean but positive values over the Asian continent and northern Africa. In climatology, the land is warmer than the ocean in summer because of the larger heat capacity of the ocean. This indicates that a stronger (weaker) land–sea thermal contrast between the tropical Indian Ocean and Asian continent in summer could enhance (weaken) the SMJ intensity and Indian summer monsoon for the high (low) ZSSTI cases. Besides, significant negative anomalies of SAT ap-

pear over the Maritime Continent and tropical western Pacific, which strengthen the land–sea thermal contrast between the western Pacific and eastern China and result in a stronger EASM in the high ZSSTI years, and vice versa. A similar feature is verified more clearly by the 850 hPa winds (Fig. 4b). Intensified CEFs near the Somali coast from the SH to NH are apparent when the ZSSTI is stronger (Fig. 4b), which is consistent with the result of positive relationships between the SMJ intensity and ZSSTI in section 3.2. In addition, there are anticyclonic anomalies located over the subtropical western Pacific along with anomalous southwesterly flow in East Asia, which means an enhanced western Pacific subtropical high coincides with a stronger EASM. It is interesting that anomalous northeasterly flow appears over the north of Australia, indicating the existence of a possible seesaw pattern between the SMJ and Australian CEFs, as recently reported by Li and Li (2014).

However, it is not clear how the dipole-like SST anomaly pattern over the southern high and middle latitudes can influence the land–sea thermal contrast over lower latitudes. To answer this question, the composite differences of the latitude–pressure cross sections of the longitude-averaged (v, ω) vector anomaly over the region from 30°E to 90°E is presented in Fig. 5a. In climatology, the ascending motion of the southern Ferrel cell is located between 50°S and 70°S, while the Hadley cell is symmetric about the equator in

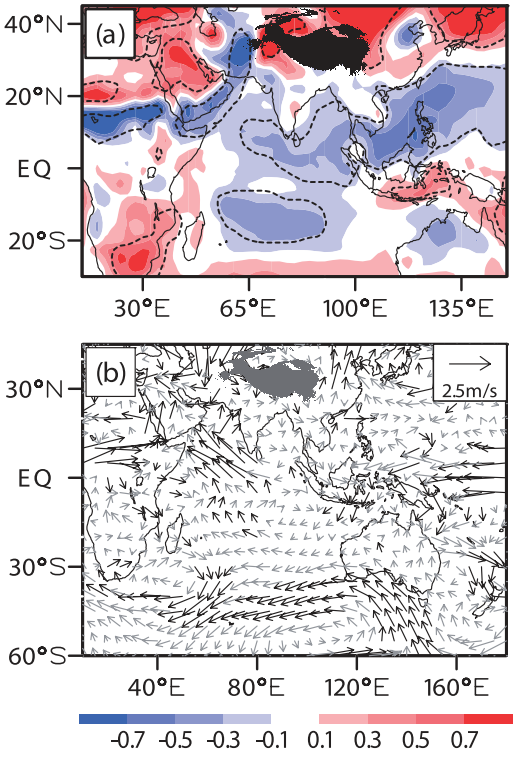

Fig. 4. Composite differences of (a) SAT (units: °C) and (b) (u, v) (units: m s^{-1}) at 850 hPa in summer between the high and low summer-ZSSTI years. Areas circled by the thick dashed curves and black bold arrows are significant values exceeding the 95% confidence level.

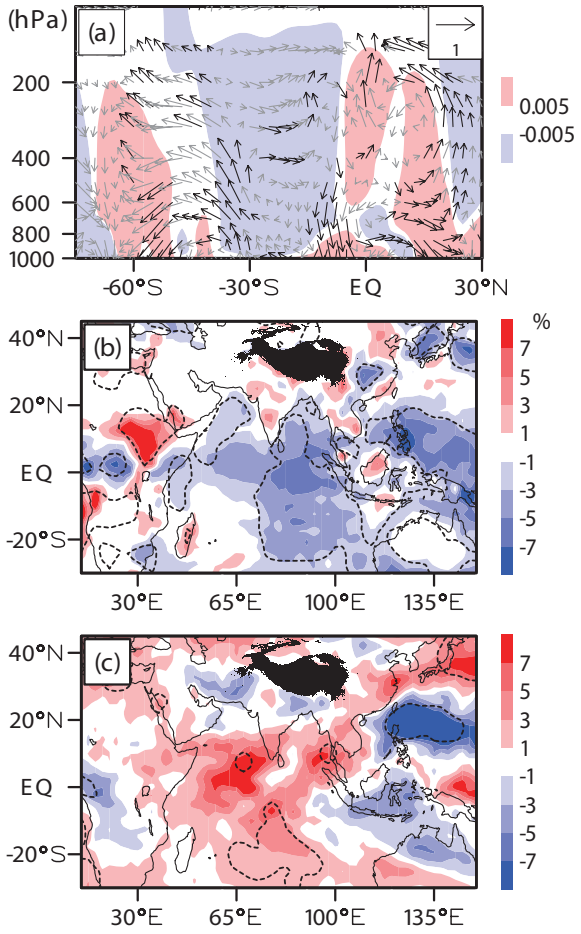

Fig. 5. Composite differences of the (a) latitude–pressure cross sections of v (units: m s^{-1}) and ω (units: hPa s^{-1}) vectors averaged between 30°E and 90°E, (b) low cloud cover (units: %) and (c) OLR (units: W m^{-2}) in summer between the high and low summer-ZSSTI years. The red (blue) coloring in (a) indicates climatological ascending (descending) motion. Areas circled by thick dashed curves and black bold arrows are significant values exceeding the 95% confidence level.

summer with its ascending motion located between 5°S and 20°N (shown by the shading in Fig. 5a). As shown in Fig. 4b, there is an anomalous anticyclone over the southwest of Australia located from 45°S to 60°S while an anomalous cyclone situated in southeastern Africa from 25°S to 40°S. It is consistent with the feature that anomalous downward and upward motions prevail in the middle–lower troposphere located near 60°S and 30°S, respectively. In other words, a warmer zonal mean SST over 30°–45°S and colder one over 50°–65°S (or in strong ZSSTI years) is conducive to a weaker regional Ferrel cell in the SH. The anomaly of the regional vertical circulation in one place should result in that at the other site. Thus, anomalous downward motion near the equator, which corresponds to the anomalous anticyclone over the Arabian Ocean in Fig. 4b, along with anomalous upward motion near 30°S and 30°N (Fig. 5a), indicate a reduced regional Hadley cell in both hemispheres (especially in the NH) for ZSSTI strong

years, and vice versa. The large-scale anomalous downward (or upward) motion may also be demonstrated by reduced (enhanced) cloud cover. The composite differences of the low cloud cover and OLR are presented in Figs. 5b and c, respectively. Negative anomalies of low cloud cover, but positive anomalies of OLR, can be seen over the tropical Indian Ocean with magnitudes of -8% and 9 W m^{-2} in the anomaly centers, respectively. This indicates that the low cloud cover and convection over tropical regions will be decreased when the ZSSTI is in strong phase, which is consistent with the anomalous downward motion near the equator in Fig. 5a. Besides, a positive anomaly in Fig. 5b but a negative one in Fig. 5c is apparent over the Asian continent, despite the values not exceeding the 95% confidence level. To some extent, this confirms the anomalous ascending motion over the latitudes of 20°–30°N in Fig. 5a. According to the interaction between clouds and radiation (Ramanathan et al., 1989, 1995; Tao et al., 1996), the clouds may absorb and reflect the solar radiation to cool the Earth's surface, while it may also absorb and emit longwave radiation to warm the Earth's surface. Therefore, the characteristics of the surface heat fluxes in the tropical Indian Ocean and Asian/African continent are analyzed in the next section to help explain the physical process responsible for the impact of the dipole-like SST anomaly pattern over the southern high and middle latitudes on the land–sea thermal contrast over lower latitudes.

At the surface, the total heating (THSRF) is given by

$$\mathrm{THSRF} = \mathrm{SWSRF} + \mathrm{LWSRF} - \mathrm{SHF} - \mathrm{LHF}; \quad (1)$$

$$\mathrm{SWSRF} = \mathrm{DSW} + \mathrm{USW}; \quad \mathrm{LWSRF} = \mathrm{DLW} + \mathrm{ULW}, \quad (2)$$

where SWSRF (LWSRF) is the net shortwave (longwave) radiation flux at the surface, SHF is the sensible heat flux, LHF is the latent heat flux (evaporation), DSW (USW) is the downward (upward) shortwave radiation flux at the surface, and DLW (ULW) is the downward (upward) longwave radiation flux at the surface.

Figure 6 shows the correlation patterns between the ZSSTI and THSRF in summer, as well as each of its components (including SWSRF, LWSRF, SHF and LHF). Here, positive fluxes indicate the Earth is absorbing heat (energy sources), while negative ones mean the Earth is venting heat (energy sinks). Climatologically, the tropical Indian Ocean releases net heat to the atmosphere and the Asian/African

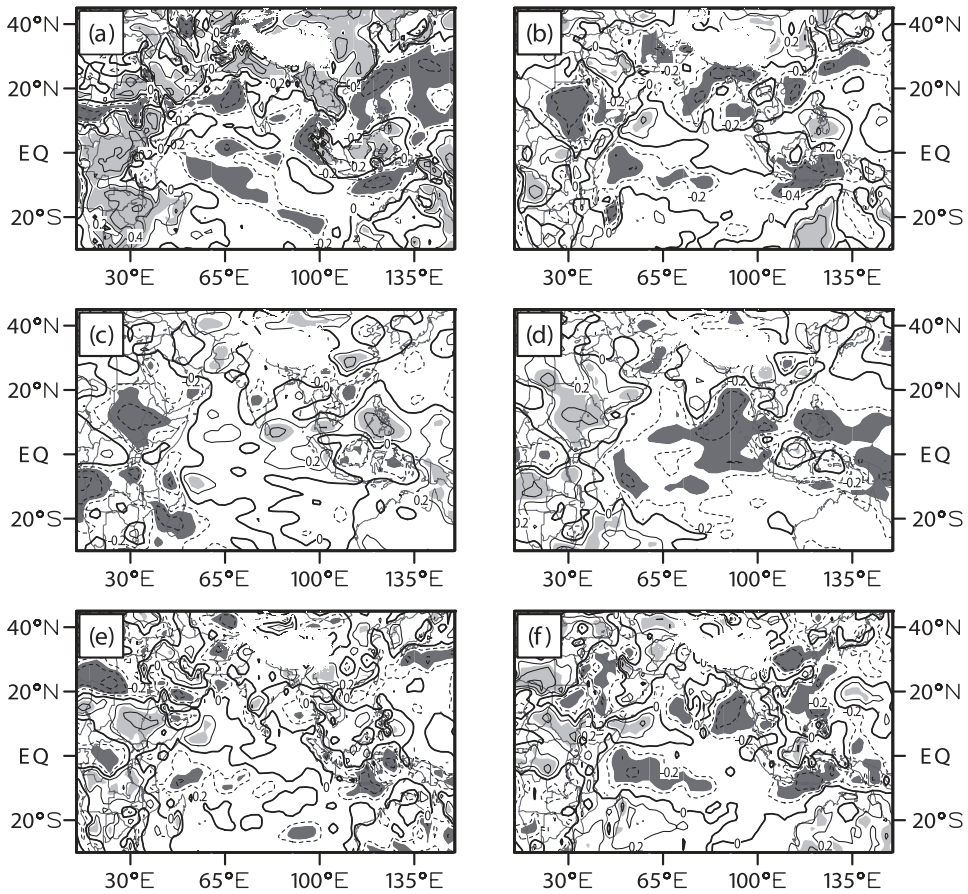

Fig. 6. Correlation patterns between the summer ZSSTI and (a) THSRF derived from the NCEP–NCAR dataset, and (b) THSRF, (c) SWSRF, (d) LWSRF, (e) SHF and (f) LHF derived from the ERA-40 dataset in summer. Positive, negative and zero contours are drawn with solid, dashed and thick lines, respectively. The intervals are 0.2. The light and dark shaded areas are significant at the 95% confidence level for positive and negative values, respectively.

continent absorbs net heat from the atmosphere in summer. As clearly revealed in Figs. 6a and b, there are significant large-scale negative correlation coefficients over the tropical Indian Ocean, Maritime Continent and tropical western Pacific, but positive ones over the Asian continent and northern Africa. This indicates more net heat is released from the tropical Indian Ocean surface (which means surface cooling), while more net heat is absorbed by the Asian/African continent surface (which means surface warming), which is consistent with the anomalous distributions of SAT, low cloud cover, and OLR in Figs. 4a, 5b and 5c. Therefore, the change in THSRF is likely responsible for the land–sea thermal contrast anomaly between the tropical Indian Ocean and Asian continent.

Next we check the anomalies of each component of THSRF to isolate the dominant contributor to the land–sea thermal contrast anomaly between the tropical Indian Ocean and Asian continent. Among them (Figs. 6c–f), LWSRF and LHF seem to be responsible for the land–sea thermal contrast anomalies. Negative correlations over the tropical Indian Ocean and positive ones over the Asian continent imply that more LWSRF and LHF are released in the tropical Indian Ocean and less LWSRF and LHF are emitted from the Asian continent. LWSRF represents a more significant contribution to land–sea thermal contrast anomalies than LHF. Meanwhile, it reflects the DLW change in Fig. 7b. No significant values exist in the correlation pattern between ULW and ZSSTI in summer (Fig. 7a). Figure 7b suggests that the decrease of DLW in the tropical ocean cools the ocean surface, while the increase of DLW over the Asian continent warms the land surface during ZSSTI positive years, in favor of the decrease of SAT over the ocean and increase of SAT over the continent. The correlation pattern of DLW with ZSSTI is collocated with composite differences of SAT anomalies in Fig. 4a and low cloud cover anomalies in Fig. 5b for high and low ZSSTI years. This demonstrates the dominant contribution of DLW to the change of land–sea thermal contrast between the tropical Indian Ocean and Asian continent and suggests that the anomalies of low cloud cover are the main cause of the longwave radiation flux change.

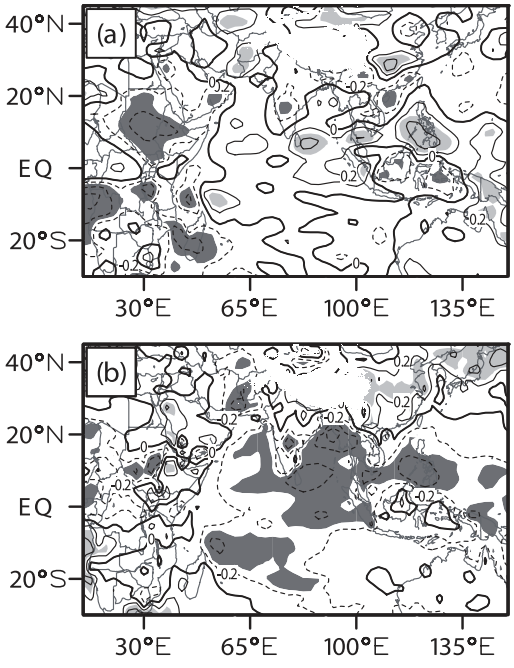

Fig. 7. As in Fig. 6 but for the (a) ULW and (b) DLW.

4.2. *Simulation experiment*

To better understand how the ocean thermal condition over the high and middle latitudes of the SH connects to the SMJ–AAO relationship, we also conduct two sensitivity experiments (referred to as pZSSTI and nZSSTI) using CAM5. Each experiment is an ensemble average of five realizations, which differ from one another in their initial conditions. In the control experiment, the monthly varying climatological SST is adopted as the sea surface boundary. The control experiment is integrated for 17 years from 1 January 1990 to 31 December 2006. Considering the model's stability, the last five years of results from the control experiment (1 January 2001–05) are selected as the five initial conditions of the pZSSTI and nZSSTI experiments. In the pZSSTI experiment, we impose a positive ZSSTI anomaly (1°C SST increase at 35°–40°S, 0.5°C SST increase at 30°–35°S and 40°–45°S; 1°C SST decrease at 55°–60°S, 0.5°C SST decrease at 50°–55°S and 60°–65°S) on the lower boundary condition used in the control experiment. The nZSSTI experiment is similar to the pZSSTI experiment, except we impose a negative ZSSTI anomaly (1°C SST decrease at 35°–40°S, 0.5°C SST decrease at 30°–35°S and 40°–45°S; 1°C SST increase at 55°–60°S, 0.5°C SST increase at 50°–55°S and 60°–65°S). As obtained by the statistical analysis, the SST anomaly in these two experiments is imposed from boreal winter to the following summer. All the simulated analyses are for the summer season.

As implemented by Wu et al. (2012, 2015), the difference of air temperature and (u, v) at 850 hPa between the with- and without-ZSSTI-anomaly experiments and their differences (pZSSTI minus nZSSTI) is presented in Fig. 8, along with the corresponding difference in simulated latitude–pressure cross sections of (v, ω) anomaly vectors averaged over 30°–90°E. In terms of air temperature at 850 hPa, positive (negative) values are located in the tropical Indian Ocean for the nZSSTI (pZSSTI) experiment (Figs. 8a and b). However, positive values cover the east of China for their differences (pZSSTI minus nZSSTI) in Fig. 8c. This implies that the land–sea thermal contrast is strengthened in strong ZSSTI years, which is basically consistent with the diagnostic result shown in Fig. 5a. For atmospheric circulation (Figs. 8d, e and 8g, h) in negative (positive) ZSSTI years, a larger scale anomalous cyclone (anticyclone) exists over the Southern Ocean near 40°–60°S and a relatively weaker anomalous anticyclone (cyclone) appears on the southeastern coast of Africa near 20°–40°S, corresponding to anomalous upward (downward) motion near 60°S and downward (upward) motions near 30°S (strengthened/weakened southern Ferrel cell for weak/strong ZSSTI cases). Besides, in tropical areas,

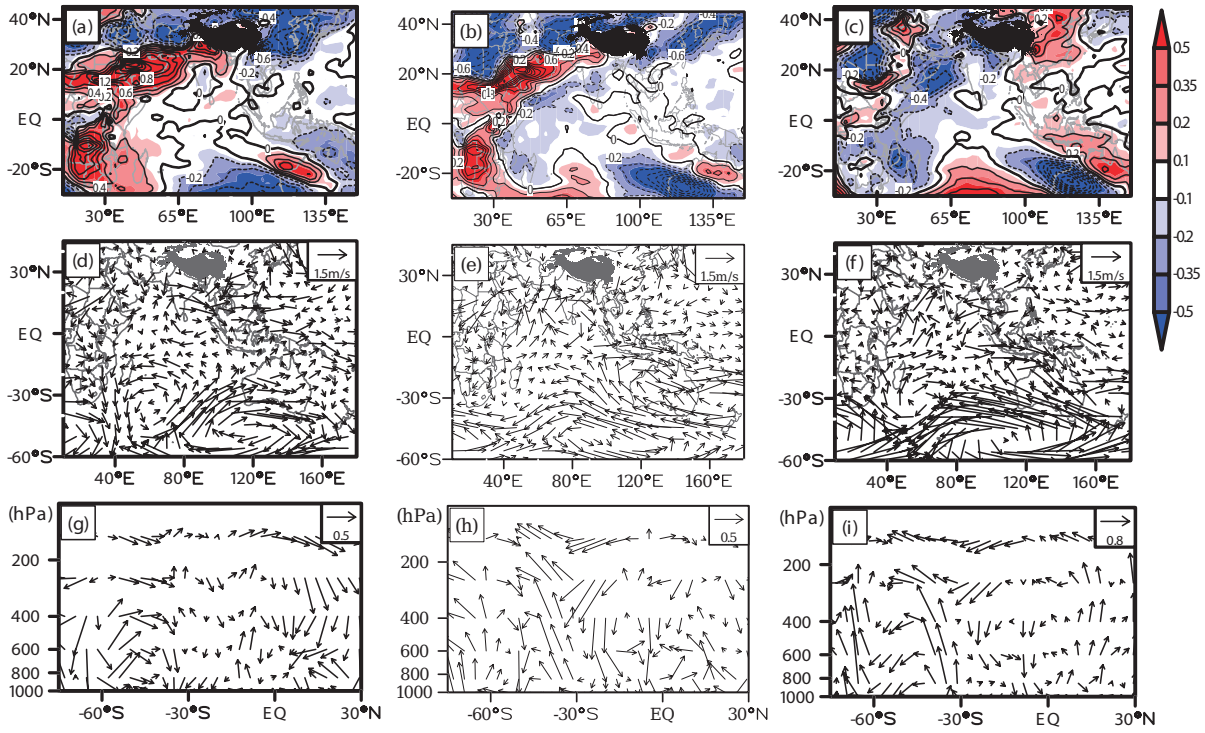

Fig. 8. Differences of (a–c) air temperature (units: °C) at 850 hPa, (d–f) (*u*, *v*) (units: m s^{-1}) at 850 hPa, and (g–i) latitude–pressure cross sections of *v* (units: m s^{-1}) and ω (units: hPa s^{-1}) vectors averaged over 30°–90°E between the with- and without-ZSSTI-anomaly experiments, as well as their differences in summer: (a, d, g) the nZSSTI experiment; (b, e, h) the pZSSTI experiment; (c, f, i) the differences between the pZSSTI and nZSSTI experiments. The contour intervals are 0.2°C.

the CEFs near the Somali coast are weakened (enhanced) dramatically and a cyclone (an anticyclone) anomaly covers the Arabian Sea, which is in agreement with the ascending (descending) motion anomaly near the equator (strengthened/weakened Hadley cell in the NH for weak/strong ZSSTI cases). These features are further verified by the differences between the pZSSTI and nZSSTI experiments in Figs. 8f and i, which are well collocated with those in Figs. 4b and 5a. It is the strong ZSSTI that activates the vertical circulation anomaly, which enhances the land–sea thermal contrast between the tropical Indian Ocean and Asian continent and causes the increased SMJ intensity for strong AAO and vice versa. To some extent, the potential physical process of the SST anomalies in the southern high and middle latitudes responsible for the SMJ–AAO relationship is confirmed by the Southern Ocean forced experiment in the CAM5 runs.

5. Summary

In this study it is found that the AAO in boreal winter has a teleconnected influence on the SMJ intensity in the following spring and summer. The teleconnected relationships are independent of ENSO. When the SMJ intensity is in a stronger positive phase, it can be traced backward to an increased SLP anomaly over the southern midlatitudes but a decreased SLP over the South Pole regions in the preceding winter, which is characterized by the positive phase of the AAO. Similar to Zheng and Li (2012), it is also found that a strong positive phase of the winter AAO is generally followed by warmer SST anomalies over the southern midlatitudes but colder SST anomalies over the southern high latitudes, and vice versa. Because the SST anomalies may persist into the following summer, the anomalous SST pattern induced by the AAO may be closely associated with the variability of the SMJ intensity. Therefore, the SST variability in the southern high and middle latitudes plays an important role in bridging the AAO and SMJ intensity.

A possible mechanism for the role of the SST variability over the southern high and middle latitudes in bridging the AAO and SMJ is also discussed. In winter, the AAO influences the SST variability in the southern high and middle latitudes through the air–sea coupling. When the AAO is in its strong (weak) phase, the Southern Ocean is anomalously warmer (cooler) in the midlatitudes but cooler (warmer) in the high latitudes, accompanied by increased (decreased) SLP over the southern midlatitudes and decreased (increased) SLP over the southern high latitudes. This anomalous SST pattern will persist from boreal winter to the following spring and summer. As Zheng and Li (2012) pointed out, the possible mechanism for this anomalous SST pattern associated with the AAO in boreal winter may be responsible for the latent heat flux change caused by the variability in sea surface wind speed. In following strong spring and summer ZSSTI years, the SST anomaly in southern high and middle latitudes activates the vertical meridional circulation anomaly with anomalous ascending motion near 30°S and descend-

ing motion near 60°S, which means a weakened local Ferrel cell. At the same time, large-scale anomalous downward motion occurs near the equator, implying a reduced regional Hadley cell (especially in the NH). The anomalous downward motion then produces a decrease in low cloud cover and downward surface longwave radiation flux over the tropical Indian Ocean, but a relative increase in low cloud cover and downward surface longwave radiation flux over the Asian continent. Consequently, less warming occurs in the tropical ocean, but more warming of the Asian continent. Finally, the land–sea thermal contrast between the tropical Indian Ocean and the Asia continent is enhanced and the SMJ intensity in summer (or spring) is also strengthened.

The mechanism discussed above is also confirmed by numerical simulation experiments based on CAM5. This is one possible way to explain the coupling of the boreal winter AAO and SMJ intensity in the following spring and summer. Other physical processes linking them are still in existence, and so further exploration of this subject is needed. This work could result in extending the lead time of seasonal forecasts of the monsoon climate from the previous spring to winter. Furthermore, in an operational setting, it should also lead to better understanding of short-term climate predictions.

Acknowledgements. We would like to thank the editor and two anonymous reviewers for improving the original manuscript. This work was jointly supported by the National Natural Science Foundation of China (Grant Nos. 41175051 and 41490642), the National Basic Research and Development (973) Program of China (Grant No. 2012CB957804), and the Postgraduate Science and Technology Innovation Project of Jiangsu Province (Grant No. CXZZ13_0517). SHI Wenjing also acknowledges the financial support of the China Scholarship Council (CSC) and constructive suggestions from Drs. Jun LI and Yun LIU, who work at the Cooperative Institute for Meteorological Satellite Studies and the Center for Climatic Research at the University of Wisconsin–Madison, USA, respectively.

REFERENCES

Carton, J. A., G. Chepurin, X. H. Cao, and B. Giese, 2000a: A simple ocean data assimilation analysis of the global upper ocean 1950–95. Part I: Methodology. *J. Phys. Oceanogr.*, **30**, 294–309.

Carton, J. A., G. Chepurin, and X. H. Cao, 2000b: A simple ocean data assimilation analysis of the global upper ocean 1950–95. Part II: Results. *J. Phys. Oceanogr.*, **30**, 311–326.

Chen, B., P. W. Guo, and Y. C. Xiang, 2005: Relationship between summer cross–equatorial flows and ENSO. *Journal of Nanjing Institute of Meteorology*, **30**, 779–785. (in Chinese)

Cong, J., Z. Y. Guan, and L. J. Wang, 2007: Interannual (interdecadal) variabilities of two cross–equatorial flows in association with the Asia summer monsoon variations. *Journal of Nanjing Institute of Meteorology*, **30**(6), 779–785. (in Chinese)

Chakraborty, A., R. S. Nanjundiah, and J. Srinivasan, 2009: Impact of African orography and the Indian summer monsoon on the low–level Somali jet. *Inter. J. Climatol.*, **29**, 983–992.

Dai, W., and Z. N. Xiao, 2014: Multi–time scale variation characteristics of Somali jet and its contact with precipitation in China. *Journal of Tropical Meteorology*, **30**(2), 368–376. (in Chinese)

Findlater, J., 1969: A major low–level air current near the Indian Ocean during the northern summer. *Quart. J. Roy. Meteor. Soc.*, **95**, 362–380.

Gruber, A., and A. F. Krueger, 1984: The status of the NOAA outgoing longwave radiation dataset. *Bull. Amer. Meteor. Soc.*, **65**, 958–962, doi: 10.1175/1520-0477(1984)065<0958:TSOTNO>2.0CO;2.

Gong, D. Y., and S. W. Wang, 1999: Definition of Antarctic oscillation index. *Geophys. Res. Lett.*, **26**, 459–462.

Gao, H., F. Xue, and H. Wang, 2003: Influence of interannual variability of Antarctic oscillation on meiyu along the Yangtze and Huaihe River valley and its importance to prediction. *Chinese Science Bulletin*, **48**, 61–67. (in Chinese)

Gao, H., Y. Y. Liu, Y. G. Wang, and W. J. Li, 2013: Precursory influence of the Antarctic Oscillation on the onset of Asian summer monsoon. *Chinese Science Bulletin*, **58**, 678–683, doi: 10.1007/s11434-012–5455–x. (in Chinese)

Halpern, D., and P. M. Woiceshyn, 2001: Somali jet in the Arabian Sea, El Niño, and India rainfall. *J. Climate*, **14**, 434–441.

Hoerling, M. P., J. W. Hurrell, T. Xu, G. T. Bates, and A. S. Phillips, 2004: Twentieth century North Atlantic climate change. Part II: Understanding the effect of Indian Ocean warming. *Climate Dyn.*, **23**, 391–405, doi: 10.1007/s00382-004–0433x.

Ho, C. H., J. H. Kin, C. H. Sui, and D. Y. Gong, 2005: Possible influence of the Antarctic Oscillation on tropical cyclone activity in the western North Pacific. *J. Geophys. Res.*, **110**, D19104, doi: 10.1029/2005JD005766.

Krishnamurti, T. N., and H. N. Bhalme, 1976: Oscillations of a monsoon system. Part I: Observational aspects. *J. Atmos. Sci.*, **33**(10), 1937–1954.

Krishnamurti, T. N., J. Molinari, and H. L. Pan, 1976: Numerical simulation of the Somali jet. *J. Atmos. Sci.*, **33**, 2350–2362.

Kalnay, E., and Coauthors, 1996: The NCEP/NCAR 40–year reanalysis project. *Bull. Amer. Meteor. Soc.*, **77**, 437–471, doi: 10.1175/1520-0477(1996)077<0437:TNYRP>2.0.CO;2.

Lei, X. C., and X. Q. Yang, 2008: Interannual variation characteristic of east hemispheric cross–equatorial flow and its contemporaneous relationships with temperature and rainfall in China. *Journal of Tropical Meteorology*, **24**(2), 127–135. (in Chinese)

Li, C., and S. L. Li, 2014: Interannual seesaw between the Somali and the Australian cross–equatorial flows and its connection to the East Asian Summer Monsoon. *J. Climate*, **27**, 3966–3981, doi: 10.1175/JCLI–D–13-00288.1.

Nan, S. L., and J. P. Li, 2003: The relationship between the summer precipitation in the Yangtze River valley and the boreal spring Southern Hemisphere Annular Mode. *Geophys. Res. Lett.*, **30**(24), 2266, doi: 10.1029/2003GL018381.

Nan, S. L., J. P. Li, X. J. Yuan, and P. Zhao, 2009: Boreal spring Southern Hemisphere Annular Mode, Indian Ocean sea surface temperature, and East Asian summer monsoon. *J. Geophys. Res.*, **114**, D02103, doi: 10.1029/2008JD010045.

Neale, R. B., and Coauthors, 2010: Description of the NCAR Community Atmosphere Model (CAM5.0), NCAR Technical Note. [Available online at http://www.cesm.ucar.edu/models/cesm1.0/cam/docs/description/cam5desc.pdf.]

Ramanathan, V., R. D. Cess, E. F. Harrison, P. Minnis, B. R. Bark-

strom, E. Ahmad, and D. Hartmann, 1989: Cloud–radiative forcing and climate: Results from the Earth Radiation Budget Experiment. *Science*, **243**(4887), 57–63.

Ramanathan, V., B. Subasilar, G. J. Zhang, W. Conant, R. D. Cess, J. T. Kiehi, H. Grassi, and L. Shi, 1995: Warm pool heat budget and shortwave cloud forcing: A missing physics? *Science*, **267**(5197), 499–503.

Rodwell, M. J., and B. J. Hoskins, 1995: A model of the Asian summer monsoon. Part II: Cross–equatorial flow and PV behavior. *J. Atmos. Sci.*, **52**, 1341–1356.

Smith, T. M., and R. W. Reynolds, 2004: Improved extended reconstruction of SST (1854–1997). *J. Climate*, **17**, 2466–2477.

Shi, W. J., and Z. N. Xiao, 2013: Variation of the cross–equatorial moisture transport in Somali and its impact on china early summer rainfall in nearly 60 years. *Meteorological Monthly*, **39**, 39–45. (in Chinese)

Shi, W. J., and Z. N. Xiao, 2014: Impact of the preceding boreal winter Southern Annular Mode on the summertime Somali Jet. *Atmos. Oceanic Sci. Lett.*, **7**, 534–539, doi: 10.3878/AOSL20140045.

Tao, W. K., S. Lang, J. Simpson, C. H. Sui, B. Ferrier, and M. D. Chou, 1996: Mechanisms of cloud–radiation interaction in the tropics and midlatitudes. *J. Atmos. Sci.*, **53**(18), 2624–2651.

Thompson, D. W. J., and J. M. Wallace, 2000: Annular modes in the extratropical circulation. Part I: Month–to–month variability. *J. Climate*, **13**, 1000–1016.

Uppala, S. M., and Coauthors, 2005: The ERA–40 re–analysis. *Quart. J. Roy. Meteor. Soc.*, **131**, 2961–3012, doi: 10.1256/qj.04.176.

Ummenhofer, C. C., A. S. Gupta, M. J. Pook, and M. H. England, 2008: Anomalous rainfall over southwest Western Australia forced by Indian Ocean sea surface temperatures. *J. Climate*, **21**, 5113–5134.

Wang, H. J., and F. Xue, 2003: Interannual variability of Somali jet and its influences on the inter–hemispheric water vapor transport and on the East Asian summer rainfall. *Chinese Journal of Geophysics*, **46**, 18–25. (in Chinese)

Wu, Z. W., J. P. Li, B. Wang, and X. H. Liu, 2009: Can the Southern Hemisphere annular mode affect China winter monsoon? *J. Geophys. Res.*, **114**, D11107, doi: 10.1029/2008JD011501.

Wu, Z., J. Li, Z. Jiang, and T. Ma, 2012: Modulation of the Tibetan Plateau snow cover on the ENSO teleconnections: From the East Asian summer monsoon perspective. *J. Climate*, **25**, 2481–2489.

Wu, Z. W., J. Dou, and H. Lin, 2015: Potential influence of the November–December Southern Hemisphere annular mode on the East Asian winter precipitation: A new mechanism. *Climate Dyn.*, **44**, 1215–1226, doi: 10.1007/s00382-014-2241-2.

Zheng, F., and J. P. Li, 2012: Impact of preceding boreal winter southern hemisphere annular mode on spring precipitation over south China and related mechanism. *Chinese Journal of Geophysics*, **55**(11), 3542–3557, doi: 10.6038/j.issn.0001-5733. (in Chinese)

Zhu, Y. L., 2012: Variations of the summer Somali and Australia cross–equatorial flows and the implications for the Asian summer monsoon. *Adv. Atmos. Sci.*, **29**(3), 509–518, doi: 10.1007/s00376-011–1120-6.